Journal of Electroanalytical Chemistry 1001 (2026) 119686

Contents lists available at ScienceDirect

Journal of Electroanalytical Chemistry

journal homepage: www.elsevier.com/locate/jelechem

Optimizing electron injection in D-A'-π-a dye sensitized solar cells: The role of electrolyte modification

Isolda Duerto [a,b], Jesús Orduna [a], Belén Villacampa [a,c], María-Jesús Blesa [a,b,*]

[a] Instituto de Nanociencia y Materiales de Aragón (INMA), CSIC-Universidad de Zaragoza, Zaragoza 50009, Spain
[b] Departamento de Química Orgánica, Universidad de Zaragoza, Zaragoza 50009, Spain
[c] Departamento de Física de la Materia Condensada, Universidad de Zaragoza, Zaragoza 50009, Spain

ARTICLE INFO

Keywords:
Driving force
Auxiliary acceptor
Redox behavior
Electrochemistry
Charge transfer
Electrolyte
Photoelectrochemical devices

ABSTRACT

This study establishes a theoretical and technical pathway, based on electroanalytical methods, for an optimized design of DSSCs with balanced short-circuit current density (J_{sc}) and open-circuit voltage parameters (V_{oc}). In this paper, isoindigo (iI) and benzothiadiazole (BTZ) are included as auxiliary acceptors in A-iI-Ph-SIL and A-BTZ-Ph-SIL dyes, respectively. The strength of auxiliary acceptors greatly influences the thermodynamic parameters governing the electron transfer process, as well as the proper distribution of electron density in orbitals. Theoretical calculations reveal that the isoindigo unit, in A-iI-Ph-SIL, exhibits a strong acceptor character that hinders charge transfer from the donor to the primary acceptor. However, in the A-BTZ-Ph-SIL, the moderate acceptor character of the benzothiadiazole unit allows charge movement across the molecule. Voltammetric analyses indicate that, in A-iI-Ph-SIL, the electron injection into the semiconductor is compromised because its excited state energy level is too close to the TiO_2 conduction band edge. This fact limits the necessary driving force for efficient injection process. To overcome this, the influence of the iodide/triiodide electrolyte composition on the electrochemical properties is explored. A concentration of 0.1 M *tert*-butylpyridine yields the optimal efficiency in these devices. This particular concentration strikes the right balance between J_{sc} and V_{oc}. Notably, this optimized concentration led to a significant 44 % improvement in DSSC efficiency compared to the conventional 0.5 M *tert*-butylpyridine concentration, achieving a maximum efficiency of 4.79 %. Electrochemical Impedance Spectroscopy indicates that better conversion efficiencies of the devices are linked to a high charge transfer resistance at the TiO_2/solvent interface.

1. Introduction

Dye sensitized solar cells (DSSCs) are described as an alternative to conventional solar cells with certain applications such as greenhouse cladding or wireless sensors due to its lightness and flexibility. [1] They are formed by a photoanode and a counter electrode assembled with an electrolyte between them. While DSSCs effectively generate high photovoltages under short-wavelength irradiation, examples of dye-sensitized solar cells sensitive to Near-Infrared (NIR) radiation remain scarce. [2] The limited NIR response of D-π-A dyes leaves a portion of the solar spectrum untapped [1] and the open-circuit voltages of devices are sometimes low due to dark current phenomena, and these dyes generally exhibit some short lifetimes. As an alternative, D-A'-π-A dyes, where A' is an auxiliary electron-withdrawing group, have emerged [3]. This group can play three roles [4]: (a) increasing the length of the π spacer, (b) improving charge delocalization, and (c) reducing the recombination. Thus, these systems allow for extending the spectral response, modulating the energy levels involved in the charge transfer process, and improving dye stability [5], giving rise to a new generation of efficient dyes [6]. Numerous examples of auxiliary acceptor systems are found, such as benzothiadiazole [5,7], benzotriazole [8], 2*H*-[1,2,3]triazolo[4,5-*c*]pyridine [9], naphthobisthiadiazole [10] and isoindigo, among others [11]. Isoindigo-based molecules have been developed for various fields of optoelectronics, such as OPVs [12,13] (Organic Photovoltaics) or OFETs (Organic Field-Effect Transistors), but in the field of DSSCs, we find few examples where this unit is used in D-A'-π-A systems [14–16]. Its use is limited maybe due to its low solubility [12]. As isoindigo exhibits the broadest absorption in the low-energy range of all the aforementioned systems [12,14,17], it was chosen as the object of study. Thus, motivated by the interest in extended absorption, the synthetic

* Corresponding author at: Departamento de Química Orgánica, Universidad de Zaragoza, Zaragoza 50009, Spain.
E-mail addresses: jorduna@unizar.es (J. Orduna), bvillaca@unizar.es (B. Villacampa), mjblesa@unizar.es (M.-J. Blesa).

https://doi.org/10.1016/j.jelechem.2025.119686
Received 26 October 2025; Accepted 24 November 2025
Available online 25 November 2025

accessibility is proposed to be improved with a C5-*N*-alkylation reaction.

A crucial aspect of the photovoltaic effect involves rapid electron injection from a photo-excited dye into the conduction band (CB) of TiO_2, followed by the regeneration of the dye and the transport of holes to the counter electrode [18]. So far, the optimization of DSSCs has primarily focused on a suite of parameters, such as light absorption and the collection of generated electrons. However, advances in electron dynamics techniques have highlighted the complexity of processes occurring at the TiO_2/dye/electrolyte interface and the importance of considering them when globally evaluating the factors affecting the efficiency of these devices. Koops, et al. [19] reported that, for the ruthenium N719 dye, the additives typically used in the liquid electrolyte have a decisive influence on the electron injection process. Specifically, both the *tert*-butylpyridine and the Li^+ are typically added to obtain the maximum V_{oc}. These additives adjust the surface charge of TiO_2 and, consequently, its conduction band, thereby acting as modulators between the energy level of the dye in the excited state and the TiO_2 conduction band [19].

This study will pave the way to design DSSCs with balanced *J-V* parameters to enhance the photovoltaic properties. In order to do that, first we propose the synthesis of a new dye, A-iI-Ph-SIL, a D-A'-π-A, system that will use the isoindigo (iI) as the auxiliary acceptor A' and will feature the *N,N'*-dialkylaniline (A) unit as the donor group. It is known that alkylanilines exhibit favorable properties, such as their simple structure, their good donor capacity, superior to triarylamines, and a high light absorption capacity [20]. This makes them alternative candidates to the commonly used donors. This aniline donor will be functionalized with an alkylsilyl group (SIL), which is expected to improve the solubility and stability of the molecules, as well as contribute to the bathochromic shift of the absorption spectrum [21]. *N*-alkylation of the nitrogen atoms in the isoindigo unit with pentyl chains, which are not explored, will be incorporated, which is expected to also improve solubility and prevent molecular aggregation [22]. The phenyl ring (pH), which will form a part of the π -unit, is expected to both reduce the recombination events [23] and stabilize the system. Finally, the cyanoacetic acid will be the acceptor and anchoring group that is expected to provide good properties to the sensitizer of these Grätzel-type cells. An analogous D-A'-π-A dye, based on benzothiadiazol, A-BTZ-Ph-SIL (Chart 1) [7], will be compared with A-iI-Ph-SIL, which also has a D-A'-π-A structure, to study the effect of the strength of auxiliary acceptors in dialkylaniline-A'-π-A dyes to find a structure-property relationship to further design new D-A'-π-A sensitizers for DSSCs. Finally, considering the strong influence of *tert*-butylpyridine (TBP) on the band edge of the conduction band of TiO_2 we proposed the modulation of this level. In order to achieve an excited state sufficiently high in energy to favor electron injection into the semiconductor, different TBP contents were explored.

2. Experimental

2.1. Synthesis and characterization

The dye A-iI-Ph-SIL, shown in Chart 1, is prepared by a convergent route (Scheme 1). The synthesis of A-BTZ-Ph-SIL was reported by [7].

2.1.1. 6,6'-Dibromo-N,N'-(1-pentyl)-isoindigo (3)

Under argon, 6,6′-dibromo isoindigo 2 (420 mg, 1.0 mmol) was dissolved in DMF. At 0 °C potassium carbonate was added (829 mg, 6.0 mmol) and the mixture was stirred for 30 min. 1-bromopentane was added dropwise at 0 °C and this mixture was heated to 100 °C for 18 h. After cooling, the DMF was evaporated. The residue was dissolved in CH2Cl2 and was washed with brine (1 × 50 mL) and with water (1 × 50 mL). The organic layer was dried with anhydrous MgSO4. The solvent was removed under reduced pressure and the residue was purified by column chromatography using silica gel (hexane/CH2Cl2 6:4) and the final product was isolated as a red solid (370 mg, 66 %).

Molecular weight (g mol^{-1}): 560.33 IR (KBr) cm^{-1}: 1597, 1687 (C=O), 2926 (Ar—H) Melting point (°C): 193 ^{1}H NMR (400 MHz, $CDCl_3$, 293 K): δ (ppm) 0.91 (t, $J = 7.2$ Hz, 6H), 1.35–1.38 (m, 8H), 1.68 (quint, $J = 7.2$ Hz, 4H), 3.71 (t, $J = 7.6$ Hz, 4H), 6.91 (d, $J = 1.6$ Hz, 2H), 7.17 (dd, $J_1 = 1.6$ Hz, $J_2 = 8.8$ Hz, 2H), 9.06 (d, $J = 8.8$ Hz, 2H) ^{13}C NMR (100 MHz, $CDCl_3$, 293 K): δ (ppm) 14.4, 22.5, 27.2, 29.2, 40.3, 111.4, 120.5, 125.2, 126.8, 131.3, 132.7, 145.9, 167.8 HMRS (ESI^+) *m/z*: calculated $[C_{26}H_{28}Br_2N_2NaO_2]$: 581.0410, found: 581.0393 $[M + Na]^+$.

2.1.2. 4-(6'-Bromo-N,N'-(1-pentyl)-isoindigo)-N-(2-((tert-butyldimethylsilyl)oxy)ethyl)-N-methylaniline (4)

To a solution of 4-bromo-*N*-(2-((*tert*-butyldimethylsilyl)oxy)ethyl)-*N*-methylaniline 1 (0.43 g, 1.25 mmol) in THF (30 mL) at −78 °C of temperature under argon atmosphere, a solution of *n*-butyllithium (1.6 M in THF) (1.27 mL, 2.03 mmol) was slowly added and it was stirred for 30 min. Then a solution of tributyltin chloride (0.4 mL, 1.5 mmol) was added and stirred for 5 min. After that, the reaction mixture was stirred at room temperature for 150 min. The reaction mixture was quenched by the addition of 50 mL of diethyl ether and the organic layer was washed with brine and dried over magnesium sulfate. After concentration under reduced pressure, the yellow residue was used without purification in the next step.

In a flask with the yellow residue solved in 22 mL of anhydrous toluene, a solution of 6,6'-Dibromo-*N,N'*-(1-pentyl)-isoindigo **3** (0.49 g, 0.87 mmol) was added. The mixture was degassed with argon during 15 min. Then Pd(PPh3)4 (0.075 g, 0.0754 mmol) was added and the

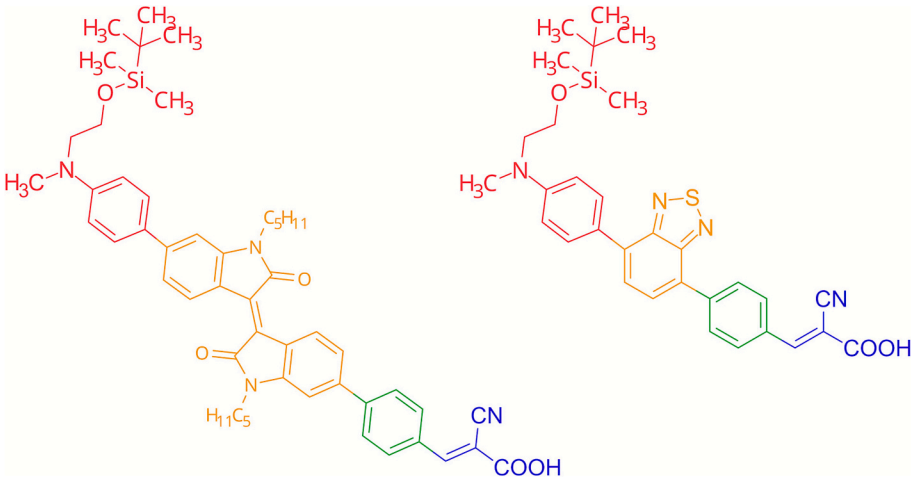

Chart 1. D-A'-π-A type dyes: **A-iI-Ph-SIL** and **A-BTZ-Ph-SIL.**

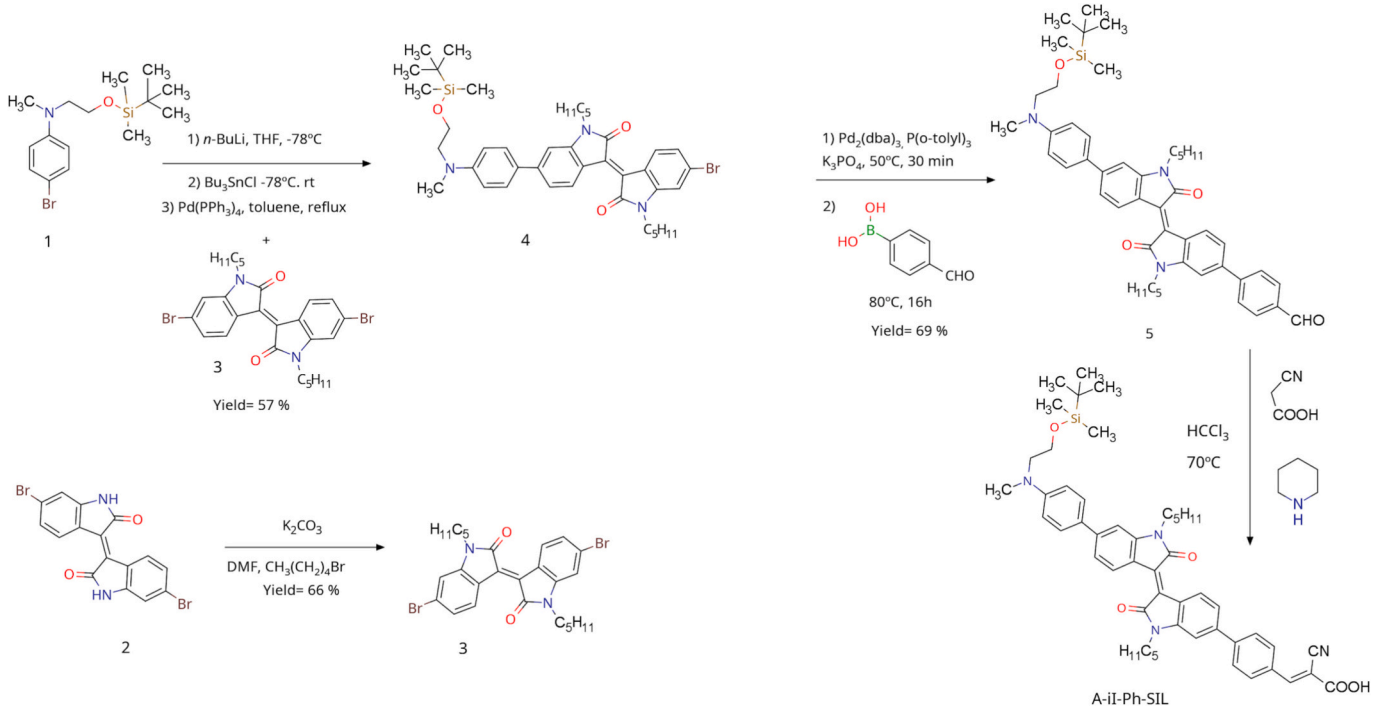

Scheme 1. Preparation of dye A-iI-Ph-SIL

mixture was heated to 100 °C for 15 h under argon atmosphere. The reaction was quenched by the addition of 66 mL of water. The mixture was extracted with toluene (2 × 60 mL). The organic layer was washed with a saturated solution of NH4Cl (1 × 60 mL) and H2O (2 × 60 mL), was dried over magnesium sulfate and the solvent was evaporated by reduced pressure. The residue was purified by flash chromatography, first with hexane/diethyl ether 94/6 to remove the and finally hexane/diethyl ether 90/10 to afford the desired as purple solid (372 mg, 57 %).

Molecular weight (g mol^{-1}): 744.88 IR (KBr) cm^{-1}: 1600, 1687 (C=O), 2931 (Ar—H) Melting point (°C): 119 ^{1}H NMR (400 MHz, $CDCl_3$, 293 K): δ (ppm) -0.04 (s, 6H), 0.89 (s, 9H), 0.90–0.94 (m, 6H), 1.35–1.39 (m, 8H), 1.72 (quint, $J = 7.2$ Hz, 4H), 3.07 (s, 3H), 3.54 (t, $J = 6$ Hz, 2H) 3.75 (t, $J = 6$ Hz, 2H), 3.78–3.85 (m, 4H), 6.78 (d, $J = 8.8$ Hz, 2H), 6.92 (d, $J = 2$ Hz, 1H), 6.94 (d, $J = 2$ Hz, 1H), 7.16 (dd, $J_1 = 2$ Hz, $J_2 = 8$ Hz, 1H), 7.24 (dd, $J_1 = 2$ Hz, $J_2 = 8$ Hz, 1H), 9.07 (d, $J = 8.4$ Hz, 1H), 9.17 (d, $J = 8.4$ Hz, 1H) ^{13}C NMR (75 MHz, $CDCl_3$, 293 K): δ (ppm) -5.2, −14.1, 22.6, 26.0, 27.3, 27.5, 28.6, 29.3, 39.4, 40.2, 40.3, 54.9, 60.6, 105.3, 111.2, 112.1, 119.6, 119.7, 120.9, 125.0, 125.7, 127.6, 128.0, 130.3, 130.6, 130.8, 145.5, 145.8, 145.9, 149.6, 168.1, 168.6 HMRS (ESI^+) *m/z*: calculated [$C_{41}H_{55}BrN_3O_3Si$]: 744.3190, found: 744.3219 $[M + H]^+$.

2.1.3. 6-(6′-(4-(N-(2-((tert-butyldimethylsilyl)oxy)ethyl)-N-methylaniline)-N, N′-(1-pentyl)-isoindigo)-benzaldehyde (5)

Compound 4 (372 mg, 0.5 mmol), $Pd_2(dba)_3$ (15 mg), P(o-tyl)$_3$ (10 mg) and K_3PO_4 (531 mg, 2.5 mmol) were dissolved in anhydrous THF in argon atmosphere. The mixture was heated to 50 °C for 30 min. A solution of 4-formylphenylboronic acid (225 mg, 1.5 mmol) in THF was added dropwise to the mixture and it was heated up to 80 °C and stirred overnight. After cooling, the crude product was extracted with dichloromethane and the organic layer was washed with brine and water. It was dried over magnesium sulfate and the solvent was evaporated by reduced pressure. The residue was purified by flash chromatography, using silica gel (hexane/AcOEt 9:1) and the final product was isolated as a purple solid (267 mg, 69 %).

Molecular weight (g mol^{-1}): 770.09 IR (KBr) cm^{-1}: 1600, 1695 (C=O), 2927 (C—H), Melting point (°C): 178 ^{1}H NMR (300 MHz, $CDCl_3$, 293 K): δ (ppm) 0.05 (s, 6H), 0.90 (s, 9H), 0.91–0.95 (m, 6H), 1.35–1.47 (m, 8H), 1.76 (quint, $J = 6.6$ Hz, 4H), 3.07 (s, 3H), 3.55 (t, $J = 6$ Hz, 2H), 3.81 (t, $J = 6$ Hz, 2H), 3.83–3.90 (m, 4H), 6.78 (d, $J = 9$ Hz, 2H), 6.95 (d, $J = 1.5$ Hz, 1H), 7.00 (d, $J = 1.5$ Hz, 1H), 7.26 (dd, $J_1 = 1.5$ Hz, $J_2 = 8$ Hz, 1H), 7.31 (dd, $J_1 = 1.5$ Hz, $J_2 = 8$ Hz, 1H), 7.57 (d, $J = 9$ Hz, 2H), 7.80 (d, $J = 8.1$ Hz, 2H), 7.98 (d, $J = 8.1$ Hz, 2H), 9.20 (d, $J = 8.4$ Hz, 1H), 9.27 (d, $J = 8.4$ Hz, 1H), 10.07 (s, 1H) ^{13}C NMR (75 MHz, $CDCl_3$, 293 K): δ (ppm) -5.2, −14.1, 22.6, 26.0, 27.5, 29.3, 39.4, 40.2, 54.9, 60.6, 105.3, 106.5, 112.1, 119.7, 121.2, 122.4, 127.6, 127.8, 128.0, 128.2, 130.2, 130.5, 130.7, 134.0, 135.8, 142.8, 145.2, 145.9, 146.7, 149.6, 168.4, 168.6, 191.9 HMRS (ESI^+) *m/z*: calculated [$C_{48}H_{59}N_3O_4Si$]: 769.4269, found: 769.4235 $[M]^+$.

2.1.4. Dye (2E)-3-{4-[(E)-6′-[4-({2-[(tert-butyldimethylsilyl)oxy]ethyl}(methyl)amino)phenyl]-2,2′-dioxo-1,1′-dipentyl-1H,1′H,2H,2′H-[3,3′-biindolyliden]-6-yl]phenyl}-2-cyanoprop-2-enoic acid, A-iL-Ph-SIL

To a solution of cyanoacetic acid (75 mg, 0.85 mmol) and piperidine (167 μL, 1.58 mmol) in dry chloroform (15 mL) a solution of the aldehyde 5 (100 mg, 0.13 mmol) was added. The mixture was heated to 70 °C of temperature for 48 h under argon atmosphere and prevented from light; then it was cooled down to room temperature. The mixture was acidified with HCl 0.1 M (20 mL) and extracted with dichloromethane (2 × 50 mL). The organic layer was washed with water (3 × 50 mL), dried over magnesium sulfate and the solvent was evaporated by reduced pressure. The resulting solid was triturated with cold pentane. The final product was isolated as a dark blue (69 mg, 63 %).

Molecular weight (g mol^{-1}): 837.13 IR (KBr) cm^{-1}: 1600, 1691 (C=O), 2221 (C≡N), 2854, 2929 (C—H), 3414 (O—H) Melting point (°C): 214 ^{1}H NMR (300 MHz, DMSO-d_6, 293 K): δ (ppm) 0.00 (s, 6H), 0.85 (s, 9H), 0.85–0.90 (m, 6H), 1.30–1.38 (m, 8H), 1.61–1.74 (m, 4H), 2.79 (s, 3H), 3.55 (t, $J = 6$ Hz, 2H), 3.77 (t, $J = 6$ Hz, 2H), 3.82–3.93 (m, 4H), 6.80 (d, $J = 9$ Hz, 2H), 7.25 (s, 1H), 7.30 (dd, $J_1 = 1.5$ Hz, $J_2 = 8.6$ Hz, 1H), 7.45 (s, 1H), 7.47 (dd, $J_1 = 1.5$ Hz, $J_2 = 8.6$ Hz, 1H), 7.57 (d, $J = 9$ Hz, 2H), 7.69 (d, $J = 9$ Hz, 2H), 8.01 (d, $J = 8.6$ Hz, 2H), 8.09 (d, $J = 8.6$ Hz, 2H), 8.20 (s, 1H), 9.14 (d, $J = 8.4$ Hz, 1H), 9.20 (d, $J = 8.4$ Hz, 1H) ^{13}C NMR insoluble HMRS (ESI^+) *m/z*: calculated [$C_{51}H_{61}N_4O_5Si$]: 837.4406, found: 837.4378 $[M + H]^+$.

2.2. Preparation of TiO_2 thin films (photoanodes)

Anodes (6 μm thick) were fabricated by screen printing TiO_2 paste (Dyesol 18NR-AO) on F-doped tin oxide (FTO, with 15 Ω sq.$^{-1}$ sheet resistance) conducting glass substrates. Prior to the deposition of the TiO_2 paste, the substrates were immersed in a solution of $TiCl_4$ (40 mM) at 90 °C for 30 min and then dried. The TiO_2 electrodes were gradually heated at 325 °C for 5 min, 375 °C for 5 min, 450 °C for 5 min and 500 °C for 15 min. The sintered TiO_2 electrodes were immersed again in a solution of $TiCl_4$ (40 mM) at 90 °C for 30 min and then washed with water and ethanol. The electrodes were heated again at 500 °C for 30 min and cooled before the soaking in the dye solution. The active area for devices was 0.25 cm^2.

2.3. Fabrication of counter electrodes

The counter electrodes were made by screen printing of Platinum paste (PT1 Dyesol) onto a conducting glass substrate (FTO, with 8 Ω sq.$^{-1}$ sheet resistance), where a small hole is made to allow the introduction of the liquid electrolyte using vacuum, followed by heating at 420 °C for 15 min.

2.4. DSSC assembly

The TiO_2 electrodes were previously activated by ozone treatment for 25 min. These films were sensitized in 0.1 mM dye solutions in THF at room temperature (optimized dye loading conditions). The sensitized electrodes were washed with THF and dried with air.

The counter electrodes by thermal treatment, 15 min at temperature of 420 °C.

Finally, sensitized electrodes and counter electrodes were sandwiched together using a thin thermoplastic sealing agent (MS004620, Dyesol) that melts at 120 °C. The classic I_3^-/I^- system was used as electrolyte (0.53 M 1-butyl-3-methylimidazolium iodide (BMII), 0.1 M lithium iodide, 0.05 M iodine and 0.52 M *tert*-butylpyridine in anhydrous acetonitrile). The devices were prepared in triplicate.

2.5. Characterization techniques

Infrared *measurements* were carried out using a Perkin-Elmer Fourier Transform Infrared 1600 spectrometer

Melting *points* were obtained on a Gallenkamp apparatus in open capillaries and are uncorrected.

NMR studies: ^{1}H and ^{13}C NMR spectra were recorded on a Bruker AV300 or ARX300 or a Bruker AV400 at 300 or 400 MHz and 75 or 100 MHz respectively; values are given in ppm (relative to TMS) and *J* values in Hz. The apparent resonance multiplicity is described as s (singlet), br s (broad singlet), d (doublet), t (triplet), q (quartet) and *m* (multiplet). ^{1}H–^{1}H COSY and ^{1}H–^{13}C-HSQC experiments were recorded on a Bruker ARX300 or a Bruker AV400 at 300 or 400 MHz in order to establish peaks assignment.

Mass Spectrometry studies Electrospray mass spectra were recorded on a Bruker Micro ToF-Q spectrometer; accurate mass measurements were achieved using sodium formate as external reference.

Optical absorption studies: UV–visible spectra were recorded with an UV–vis Cary 6000. Absorption runs were carried out with films and solutions 10^{-4}–10^{-5} M THF.

On the one hand, the evolution of electrode absorption was tracked as a function of soaking time: TiO_2 photoanodes were immersed in the dye solution for progressively longer times until absorption saturation was observed. We used semi-transparent photoanodes, ensuring their similarity in thickness and roughness, to establish the optimal immersion times for cell preparation.

On the other hand, the amount of dye adsorbed on the surface of TiO_2 anode was estimated. For dye desorption, a NaOH 10^{-3} M H_2O/THF (20:80) solution was used. The concentration of the desorbed dye solutions was subsequently quantified using UV–Vis absorption.

Pulse differential voltammetry measurements were performed with a μ-Autolab type III potentiostat using a glassy carbon working electrode, Pt counter electrode, and Ag/AgCl reference electrode. The experiments were carried out under argon in THF, with Bu4NPF6 as supporting electrolyte (0.1 mol L^{-1}). Scan rate was 0.01 V s^{-1}, modulation amplitude 0.025 V and modulation time 0.05 s^{-1}.

2.6. Photovoltaic performance measurements

The *J/V* curves of the cells were recorded using a solar simulator (Abet Technologies model 10,500) equipped with a 150 W xenon lamp. The illumination intensity was measured to be 100 mW cm^{-2} with a calibrated silicon reference cell (by ReRa). The appropriate filters (KG5) were utilized to faithfully simulate the AM 1.5G spectrum. The applied potential and cell current were measured using a Keithley 2401 digital source meter.

The IPCE (incident photon to current conversion efficiency) was measured using a home-made set up consisting of a 150 W xenon lamp, a motorized monochromator and a Keithley 2401 digital source meter.

Electrochemical impedance spectroscopy (EIS) measurements were performed in the frequency range from 0.1 to 10^5 Hz. A potentiostat (Autolab Type III) equipped with a Frequency Response Analysis (FRA) module was employed for these measurements. The solar simulator described above was used for all measurements under illumination.

3. Results and discussion

3.1. Synthesis and characterization of dyes

The A-iI-Ph-SIL dye is prepared by a convergent route (Scheme 1) which starts with the aniline 1 and the isoindigo derivative 2.

On the one hand, the aniline-based donor 1 was synthesized by two consecutive reactions: the bromination of the commercial 2-(methylphenylamino)-ethanol and the subsequent formation of aniline alkoxide, which reacts with chloride of *tert*-butyldimethylsilyl [10].

On the other hand, an aldol condensation and subsequently the dehydration of 6-bromoisatin and 6-bromooxoindole in acetic acid allowed the synthesis of the auxiliary acceptor unit A', 6′-dibromoisoindigo 2. [24]. This product 2 was *N*-alkylated with pentyl bromide, and with the aim of increasing solubility and avoiding intra- and intermolecular interactions [14], and the product 3 was obtained.

A Stille coupling [25] between this product 3 and the stannane of compound 1 was carried out and the product 4 was obtained (due to its instability, the organostannan intermediate was used in the next step without purification).

Aldehyde 5 was synthesized using a Suzuki coupling between 4-formylphenylboronic acid and compound 4 using a palladium catalyst together with a bulky tolylphosphine and K_3PO_4 as a base [14]. This aldehyde incorporates a phenyl ring to reduce planarity.

Finally, this A-iI-Ph-SIL dye was obtained by a Knoevenagel condensation with cyanoacetic acid in the basic medium following the method described in literature [26]. ^{1}H and ^{13}C NMR spectra of these synthetized compounds are reported in Supporting Information (Figs. A.1 – A.12).

The synthesis details of the A-BTZ-Ph-SIL dye can be found in [7].

3.2. Optical measurements

We investigated the optical and electrochemical properties of the dyes A-iI-Ph-SIL to determine their suitability as sensitizers for DSSCs. The UV–Vis optical absorption of these dyes measured in THF solution ($1{\cdot}10^{-4}$ M) are shown in Fig. 1. A-iI-Ph-SIL shows enhanced and broader absorption characteristics compared to A-BTZ-Ph-SIL [7]. For compound A-iI-Ph-SIL, two absorption bands were observed in the visible region. The first band, around 400 nm, is assigned to the transition $\pi \rightarrow \pi^*$. The

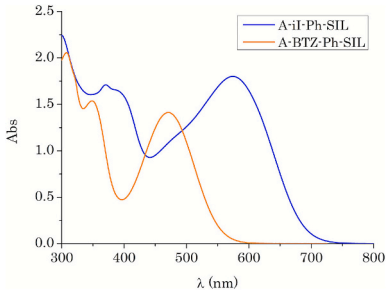

Fig. 1. UV–Vis spectra of dyes A-iI-Ph-SIL and A-BTZ-Ph-SIL [7].

second one, which corresponds to the charge transfer transition between the donor and the acceptor, has the maximum at λ_{max} = 575 nm. The charge transfer band of A-BTZ-Ph-SIL dye extends between 400 and 550 nm, and is hypsochromically shifted with respect to A-iI-Ph-SIL.

To determine the molar extinction coefficient, optical absorption spectra were measured for solutions in the range $2{\cdot}10^{-5}$ - $1{\cdot}10^{-4}$ observing a linear dependence of absorbance on concentration throughout the entire range. (Supporting Information, Fig. A.13). Table 1 shows the value of the absorption maxima wavelengths and the extinction coefficient of both dyes.

Moreover, UV–Vis absorption measurements were carried out on the sensitized TiO_2 films with the aim to optimize the immersion time of the anode and also to control any aggregation phenomena. The existence of aggregates generally produces a broadening of the absorption band on TiO_2 by increasing time, hence the importance of taking measurements at different immersion times. The sensitized anodes were measured after different immersion times, 2.5 h, 5 h and 8 h, in 0.1 mM dye solution. Fig. 2-left illustrates that for A-iI-Ph-SIL dye the maximum adsorption was achieved after 5 h of immersion. As shown in Fig. 3-left, the absorbance of the A-BTZ-Ph-SIL dye exhibited a clear trend towards saturation within 8 h of immersion. Further investigation revealed that increasing the immersion time to 24 h did not lead to a significant increase in the absorbance.

The normalized spectra (Figs. 2-right and **3**-right) show a hypsochromic shift due to dye anchoring when comparing solutions to films. However, we observed no broadening or shifting of the absorption band in films over immersion time. Hence, we can say that aggregation phenomena do not take place after 8 h as inmersion time, then this time was chosen for immersion of the TiO_2 anode in dye solutions.

3.3. Electrochemical measurements

The electrochemical properties of the dye A-iI-Ph-SIL was studied by differential pulse voltammetry (DPV) in THF solution 1 10^{-4} M (Fig. A.14). The values obtained are shown in Table 2. The potential values of the levels involved in the charge transfer process, are of great importance, since their values will determine both the capacity of electronic injection of the dye to the semiconductor and the regeneration of the dye once it has been oxidized.

The oxidation potential of a dye, *Eox*, corresponds to the oxidation of the donor, in this case, the *N,N'*-dialkylaniline. Since A-iI-Ph-SIL and A-BTZ-Ph-SIL have the same donor unit, similar values were expected. In this case, a value of E_{ox} = +1.13 V is obtained for both dyes (Fig. A.14, in Supporting Information and [7], respectively), which is more positive than the one associated with pair I_3^-/I^- (+0.4 V vs. NHE). Consequently, we can say that A-iI-Ph-SIL and A-BTZ-Ph-SIL can be effectively regenerated once oxidized, capturing electrons from the redox couple I_3^-/I^- present in the electrolyte (Supporting Information, Fig. A.15). However, very different values were obtained for $E_{0\text{–}0}$, the energy involved in the transition between the ground and first excited states (also known as the energy gap). These values were calculated by taking the intersection of the tangent to the low-energy side of the absorption spectrum with the abscissa axis. The dye with the isoindigo unit as A', A-iI-Ph-SIL, has a noticeably smaller energy gap ($E_{0\text{–}0}$ = 1.78 V) than A-BTZ-Ph-SIL ($E_{0\text{–}0}$ = 2.24 V). These very different values significantly influence the excited state oxidation potential (E^*_{ox}) of each dye. For A-BTZ-Ph-SIL, the difference between its E_{ox} and the conduction band edge of TiO_2 (−0.50 V) is sufficient to ensure the electron transfer from the dye to the semiconductor (Supporting Information, Fig. A.15). On the contrary A-iI-Ph-SIL's E_{ox} is too close to the TiO_2 CB edge, with a difference of only 0.15 V. This is less than the 0.2 V threshold, usually considered a requirement for efficient electron transfer. Consequently, electron injection from A-iI-Ph-SIL into the semiconductor may be hampered, leading to low photocurrent values in cells based on this dye.

Table 1
Optical parameters of dyes A-iI-Ph-SIL and A-BTZ-Ph-SIL.

Dyes	λ^a (nm)	λ^b (nm)	$\varepsilon{\cdot}10^{-4}$ (M^{-1} cm^{-1})
A-iI-Ph-SIL	575	554	1.76 ± 0.01
A-BTZ-Ph-SIL [7]	471	448	1.44 ± 0.05

[a] THF solution.
[b] TiO_2 film.

3.4. Theoretical calculations

The theoretical calculations were used as a tool to study the charge transfer of the molecules. The optimization of the geometry of the ground state, the first excited state and the radical cation formed after the loss of an electron were studied by DFT. From the fundamental state, both the wavelength of maximum absorption and the oscillator strength, *f*, were calculated. The latter is related to the molecular absorption of light. The oxidation potential of the ground state, E_{ox}, was obtained from the difference between the Gibbs free energy (ΔG) of the neutral species and that of the radical cation. The energy of the transition, $E_{0\text{–}0}$, is calculated as the energy difference between the first excited state and the ground state in its optimized geometry. Finally, the oxidation potential of the excited state is estimated taking into account the oxidation potential of the fundamental state and $E_{0\text{–}0}$.

The computational analysis on A-iI-Ph-SIL reveals a low excitation energy that corresponds to the intramolecular transfer of one electron from the HOMO to the LUMO. The distribution of the frontier orbitals is useful to understand the optoelectronic properties of these dyes because they are related to both their charge transfer and optical properties [27]. Fig. 4 depicts the distribution of HOMO and LUMO orbitals involved in the electron transfer of the A-iI-Ph-SIL dye. It is observed that the HOMO orbital is located on the aniline moiety, the donor part of the molecule, with an extension into the adjacent phenyl ring. The LUMO orbital is mainly located in the central area of the isoindigo unit and no significant electron density is appreciated in the acceptor and anchor group of the molecule. This scarce electron distribution of the LUMO orbital in the part of the dye that interacts with the semiconductor, together with the poor overlap observed between the orbitals HOMO and LUMO, suggests that the device with A-iI-Ph-SIL will exhibit low photocurrent values, since electron injection is seriously hampered [28].

Comparison of the molecular properties listed in Table 3 with experimental data in **Tables 1 and 2** reveals good agreement. Specifically, excellent approximations were obtained for the E_{ox} and $E_{0\text{–}0}$ values, with a reasonable estimation for the E^*_{ox} value. The E^*_{ox} value for A-iI-Ph-SIL estimated by DFT is energetically close to the CB edge of TiO_2, which is suboptimal for ensuring efficient electron injection. Likewise, computational studies on the A-BTZ-Ph-SIL dye [7] also indicated that the charge transfer band corresponds to an intramolecular electron transfer from the HOMO to the LUMO. The HOMO orbital is fundamentally located in the donor part of the molecule, extending towards the benzothiadiazole ring. LUMO extends from the auxiliary acceptor BTZ to the acceptor and anchoring group of the molecule. This extended LUMO distribution facilitates its effective overlap with

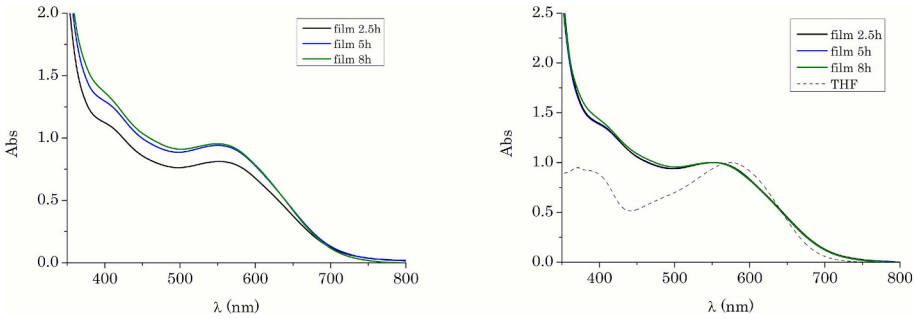

Fig. 2. a) UV–Vis spectra of photoanodes sensitized with A-iI-Ph-SIL after 2.5 h, 5 h and 8 h immersion (left); b) Normalized UV–Vis spectra of A-iI-Ph-SIL film and solution (right).

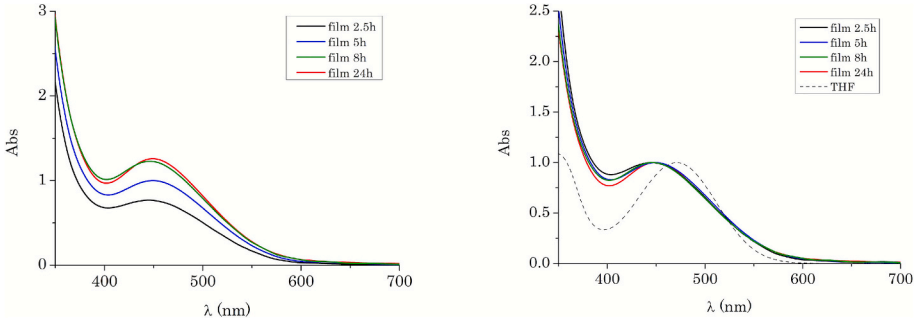

Fig. 3. a) UV–Vis spectra of photoanodes sensitized with A-BTZ-Ph-SIL after 2.5 h, 5 h and 8 h immersion (left); b) Normalized UV–Vis spectra of A-BTZ-Ph-SIL film and solution (right).

Table 2
Electrochemical properties of dyes A-iI-Ph-SIL and A-BTZ-Ph-SIL [7].

Dye	Eox^{a} (V)	λ_{cut} (nm)	$E_{0\text{-}0}{}^{b,c}$ (eV)	$(E_{ox}{}^{*})^{c,d}$ (V)
A-iI-Ph-SIL	1.13	697	1.78	−0.65
A-BTZ-Ph-SIL	1.13	554	2.24	−1.11

[a] E_{ox} vs NHE = E_{ox} (DPV, Ag/AgCl) +0.199.
[b] $E_{0\text{-}0} = 1239.84/\lambda$cut
[c] E^{*}_{ox} vs NHE = E_{ox}- $E_{0\text{-}0}$.

conduction band edge, leading to more efficient electron injection into the CB [29] compared to the A-iI-Ph-SIL dye.

To understand the role of auxiliary acceptors (A') in these D-A'-π-A systems, computational chemistry offers tools like Natural Population Analysis (NPA) [30]. NPA provides crucial information on charge distribution and the origin of electron transfer within these systems [31]. Thus, NPA analysis was performed using the M06-2× functional on the optimized geometries of both the ground state and the excited state for A-iI-Ph-SIL and A-BTZ-Ph-SIL dyes. The results are shown in Table 4.

The analysis of these charges in the ground state (S_0) indicates the molecule's polarization. The donor group, alkylaniline, has a positive value, confirming its electron-donating nature. The positive value also obtained for the phenyl ring, which acts as a π-spacer, demonstrates that

Table 3
Calculated optical and electrochemical properties of dyes A-iI-Ph-SIL and A-BTZ-Ph-SIL.

Dye	$\lambda_{max}{}^{a}$ (nm)	f^{b}	E_{HOMO} (eV)	E_{LUMO} (eV)	$E_{0\text{-}0}$ (eV)	Eox^{c} (V)	$(E_{ox}{}^{*})^{c,d}$ (V)
A-iI-Ph-SIL	526	1.19	−6.50	−2.57	1.92	1.12	−0.80
A-BTZ-Ph-SIL	443	1.12	−6.59	−2.28	2.35	1.13	−1.22

[a] Calculated M06-2×/6–311 + g(2d,p). Solvation Model CPCM, CH_2Cl_2.
[b] *f* oscillator strength
[c] vs NHE
[d] Excited stated oxidation potential vs NHE, $(E_{ox})^{*}$=E_{ox}-$E_{0\text{-}0}$.

Table 4
Calculated NPA charges for the different units and charge difference between the states of the D-A'-π-A dyes, A-iI-Ph-SIL and A-BTZ-Ph-SIL, in the ground state and in the excited state.

Dye	State	D	A'	π	A
A-iI-Ph-SIL	S_o	+0.049	−0.034	+0.072	−0.087
	S_1	+0.218	−0.169	+0.061	−0.110
	Δq	+0.169	−0.135	−0.011	−0.023
A-BTZ-Ph-SIL	S_o	+0.062	−0.052	+0.079	−0.089
	S_1	+0.469	−0.262	+0.020	−0.227
	Δq	+0.407	−0.210	−0.059	−0.138

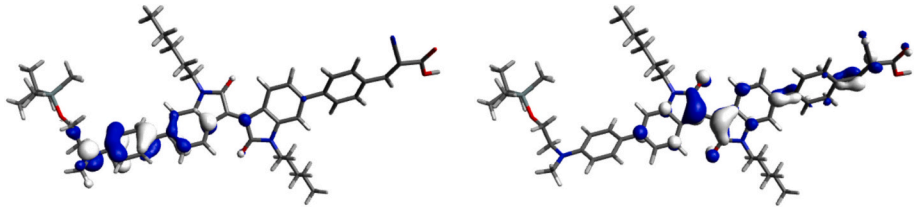

Fig. 4. Molecular orbitals HOMO (left) and LUMO (right) of A-iI-Ph-SIL dye.

this unit facilitates electron transport from the donor to the acceptor. Since the donor and acceptor are common in both dyes, A-iI-Ph-SIL and A-BTZ-Ph-SIL, similar NPA charge values are obtained for these parts of the molecule in the ground state. The negative charges obtained for isoindigo, A', and the cyanoacetic acid acceptor, A, confirm their role as electron-withdrawing groups.

As can be seen in Table 4, the charge difference (Δq) from the ground state (S_0) to the excited state (S_1) in the different parts of the molecule informs about the charge transfer [32,33] and the results obtained are revealing. On the one hand, the charge donated by the aniline (D) in the A-BTZ-Ph-SIL dye is more than double than that from the A-iI-Ph-SIL dye. On the other hand, the charge accepted by the cyanoacetic acid is six times greater in the A-BTZ-Ph-SIL dye than in the A-iI-Ph-SIL dye. This leads us to conclude that the isoindigo unit hinders charge transfer to the anchoring site. Most of the negative charge is retained, and virtually no increase in charge is observed in the cyanoacetic anchor group. This result is consistent with what has already been observed and corroborates the low electron density in this region of the molecule. In contrast, in the case of A-BTZ-Ph-SIL, the charge loss from the donor group is distributed between the π spacer and the acceptor groups A' and A, whose negative charge indicates that they are capable of efficiently extracting electrons trapped in the molecular structure. Consequently, during the photoexcitation process, the electrons from the donor group of the A-BTZ-Ph-SIL dye would be transferred to the acceptor group, so that BTZ, in this case, allows the movement of charge to the anchor group.

This charge transfer that occurred during the transition from the ground to the excited state of the dye can be visualized using electron density difference maps (EDDM). [34] These representations allow the charge transfer associated with a transition to be indicated using a color code. Blue indicates the area of maximum electron density loss, while red indicates the area of maximum gain. The EDDM has been plotted for both dyes in the transition to the first excited state (Fig. 5). In A-iI-Ph-SIL, the charge accumulation is again observed in the isoindigo unit, which acts as an electron trap, with a more intense red color in this unit (Fig. 5, left). In contrast, in the A-BTZ-Ph-SIL dye (Fig. 5, right), the charge loss in the donor unit (aniline) is gained in both A' (benzothiadiazole) and A (cyanoacetic acid). The slight blue coloration in the BTZ unit confirms that, despite its electrowithdrawing nature, it allows electron transfer from the donor to the acceptor. Therefore, better photovoltaic properties are expected for the A-BTZ-Ph-SIL dye than for A-iI-Ph-SIL.

3.5. Photovoltaic measurements

To evaluate the potential of the A-iI-Ph-SIL dye as a sensitizer in DSSCs, a preliminary approach was taken. The electrolyte based on the redox couple I_3^-/I^- with the standard concentrations was used: BMII (0.5 M), LiI (0.1 M), I_2 (0.05 M) and TBP (0.5 M) [35] The TiO_2 photoanodes (6 μm thick) were sensitized in a 0.1 mM THF solution. UV–vis studies (Section 2.2) have shown that photoanodes with the isoindigo dye have an optimal immersion time of 5 h, but no deterioration is observed with an immersion time of 8 h. Hence this immersion time was chosen for both dyes, A-iI-Ph-SIL and A-BTZ-Ph-SIL, in order to build the devices under the same conditions and all in triplicate.

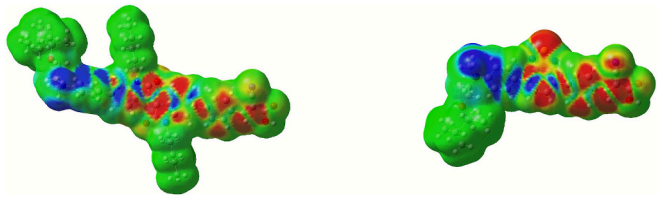

Fig. 5. Electron density difference maps for A-iI-Ph-SIL (left) and A-BTZ-Ph-SIL (right).

Devices with the A-BTZ-Ph-SIL dye (Supporting Information, Table A.1) demonstrated an efficiency of 5.73 % (J_{sc} = 13.8 mA/cm^2, V_{oc} = 0.638 V, ff = 63.9 %). This signifies a 33 % enhancement over the earlier reported 4.30 % (10.26 mA/cm^2, 0.630 V, 66.0 %) [7]. In that study, the cells were prepared using photoanodes sensitized by immersion in dichloromethane solutions (8 h) of the dye with photoanodes 6 and 8 μm thick, repectively. However, tetrahydrofuran (THF) was employed as the solvent in this case, due to the A-BTZ-Ph-SIL dye's higher solubility. In these conditions, the photovoltaic performance of the A-iI-Ph-SIL dye was characterized (Table 5) yielding an efficiency of 3.32 % (J_{sc} = 9.01 mA/cm^2, V_{oc} = 0.560 V, ff = 65.8 %). As predicted, the photocurrent of devices utilizing this dye (9.01 mA/cm^2) was lower than the value reported above for the dye with BTZ as the auxiliary acceptor (13.80 mA/cm^2). For the A-iI-Ph-SIL dye, the proximity of its E_{ox}^* to the TiO_2 CB edge, combined with the poor electron density of the LUMO orbital at the acceptor and anchoring group, negatively impacts the device's performance by reducing electron injection efficiency.

Taking into account the influence of TBP on the conduction band edge and, concomitantly, on its Fermi level [36], we are going to consider different TBP contents to modulate this level and in order to achieve an excited state sufficiently high in energy to favor electron injection into the TiO_2 while maintaining V_{oc}. As we are going to see, this TBP modulation on the electrolyte will provide an optimization of the efficiency that constitutes one of the main results of this paper.

3.5.1. Effect of different concentrations of TBP on the I_3^-/I^- electrolyte

TBP has two opposite effects on the photovoltaic parameters. The decrease in TBP concentration leads to an increase in J_{sc}, but the V_{oc} is simultaneously affected negatively. Several authors have reported studies on DSSCs based on isoindigo dyes, where the electrolyte used contained *tert*-butylpyridine (TBP) at concentrations lower than typical (0.5 M) [37,38], or even completely eliminated [11,14,16]. In this case J_{sc} is improved since electron injection is favoured, because the CB of TiO_2 is shifted to more positive potential values [38] (Fig. 6**).** On the other hand and at the same time, higher content of TBP improves the V_{oc}, contributing to enhance the solar cell efficiency. This phenomenon stems from TBP's Lewis basicity character and its ability to coordinate to the TiO_2 surface via the lone electron pair on its nitrogen atom, thereby inducing a dipole [19]. Then, it is necessary to find a trade-off between the two parameters [39].

For this purpose, firstly a TBP-free I_3^-/I^- electrolyte was used. To compare the behavior of these D-A'-π-A systems, photovoltaic devices based on both dyes were built under the same conditions: 6 μm thick electrodes were immersed for 8 h in 0.1 mM THF solutions of each dye.

These measurements were compared with those obtained using the standard electrolyte (0.5 M TBP). This electrolyte typically yields optimal performance for dyes with suitable energy levels, such as A-BTZ-Ph-SIL, as it meets the thermodynamic requirements for efficient charge

Table 5
Average values, experimental uncertainty of the measured photovoltaic parameters and best value in brackets: open circuit voltage (V_{oc}), short circuit current density (J_{sc}), fill factor (ff) and overall efficiency (η). Three cells of each type were prepared and characterized. (Experimental conditions: 6 μm thick photoanode of Dyesol 18NR-AO (paste). 0.1 mM THF A-iI-Ph-SIL solution. Cell area tested: 0.25 cm^2. 24 h after self assembly.

[TBP] (M)	J_{sc} (mA/cm^2)	V_{oc} (V)	Ff (%)	η (%)
0	14.08 ± 0.17 (14.1)	0.440 ± 0.005 (0.440)	56.8 ± 0.4 (57.8)	3.52 ± 0.07 (3.59)
0.1	12.80 ± 0.20 (13.0)	0.598 ± 0.008 (0.590)	61.6 ± 0.6 (62.3)	4.73 ± 0.17 (4.79)
0.3	10.90 ± 0.10 (11.1)	0.575 ± 0.012 (0.578)	64.0 ± 0.9 (62.9)	4.02 ± 0.19 (4.11)
0.5	9.00 ± 0.01 (9.01)	0.568 ± 0.008 (0.560)	64.9 ± 0.9 (65.8)	3.31 ± 0.09 (3.32)

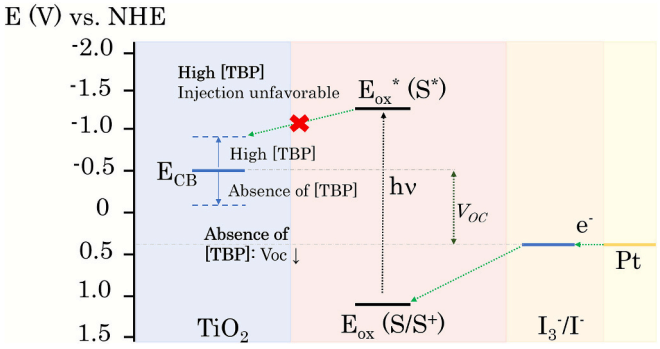

Fig. 6. Conduction band edge (E_{CB}) shift of TiO_2 with the concentration of *tert*-butylpyridine [TBP].

injection in DSSCs.

Fig. 7-**left** presents the *J-V* curves obtained for cells incorporating both dyes and both electrolyte configurations. The use of TBP-free electrolyte yields to efficiency values of 3.59 % (14.1 mA/cm^2 0.440 V, 57.8 %) and 3.70 % (14.1 mA/cm^2, 0.500 V, 52.6 %) for A-iI-Ph-SIL (Table 5) and A-BTZ-Ph-SIL (Supporting Information, Table A.1), respectively.

For the A-iI-Ph-SIL dye (see Table 5), even with the significant improvement in the injection process, the absence of *tert*-butylpyridine (TBP) led to a notable 120 mV decrease in the V_{oc} values. This is due to the shifting of the CB edge of TiO_2 towards more positive values, which reduces the energy difference between the CB edge and the electrolyte's redox potential. This difference is directly related to the V_{oc} parameter. Despite this decrease, the significant increase in photocurrent (J_{sc}) still led to an 8 % improvement in the overall efficiency of these DSSCs. However, for A-BTZ-Ph-SIL devices (Supporting Information, Table A.1), the short-circuit current values remain essentially unchanged from reference conditions (TBP 0.5 M), indicating that injection is unaffected. The value of the oxidation potential of the excited state providing a sufficient driving force, ensures adequate electron injection into the semiconductor minimizing the TBP effect.

The limited impact of TBP's absence on cells with the A-BTZ-Ph-SIL dye was also reflected in the IPCE curve (Fig. 7-**right**), which was similar across both electrolyte configurations, reaching an $IPCE_{max}$ of ~70 % and spanning a spectral range of 400 to 600 nm. Conversely, for the A-iI-Ph-SIL dye, both IPCE curves are clearly different, reaching an $IPCE_{max}$ of 55 % with the TBP-free electrolyte. It is observed that the use of isoindigo extended the range of photon-to-current conversion up to 700 nm.

Additionally, to investigate if aggregation played a role in the A-iI-Ph-SIL dye's performance in the absence of *tert*-butylpyridine, devices were also constructed using CDCA as an antiaggregant. No improvement was observed (J_{sc} = 14.3 mA/cm^2, V_{oc} = 0.425 V, *ff* = 57.2 %, η = 3.47 %), which reaffirms that the introduced C5 chains in this dyes effectively prevent aggregation phenomena, as previously predicted by UV–Vis spectroscopy (Fig. 2).

The stability of the devices over time was assessed through intermittent measurements of their photovoltaic parameters, extending beyond 1000 h post assembly. Fig. 8 summarizes the obtained results.

Regarding the A-iI-Ph-SIL dye (Fig. 8 left), we observe that V_{oc} remains stable. However, the J_{sc} value and the overall device efficiency decrease. Low stability is one of the major drawbacks of near-NIR dyes and is usually associated with either the formation of aggregates or with the loss of directionality of the excited state, [40–42] which could be related to our situation with the strong acceptor character of **iI**. As it has been previously described [43] this decrease is more pronounced in devices that do not contain *tert*-butylpyridine since this additive helps increase their temporal stability due to the low position of the semiconductor's conduction band (Fig. 6). However, the efficiency of A-BTZ-Ph-SIL dye (Fig. 8**,** right) is stable over the evaluated period. The small decrease in J_{sc} can be due to both the neutralization of Li^+ ions and the adsorption of *tert*-butylpyridine on the TiO_2 surface. These processes induce a shift of the CB edge to more negative values, leading to an increase in V_{oc} accompanied by a loss of photocurrent. Due to this opposing balance of effects, the overall efficiency is found to remain stable.

Considering the observed results, and with the aim of maximizing the efficiency of the A-iI-Ph-SIL dye, additional series of devices were constructed by exploring other *tert*-butylpyridine concentrations in the range between 0 and 0.5 M. Thus, TBP was added at concentrations of 0.1 and 0.3 M, maintaining the usual concentrations of the other components (BMII 0.5 M, LiI 0.1 M, and I_2 0.05 M). Fig. 9-**left** displays the *J-V* curves for these conditions, alongside those at 0 M and 0.5 M. The comparison of photovoltaic parameters for DSSCs with the four explored electrolyte configurations can be seen in the Table 5**.**

It was evident from these results that electrolyte composition clearly impacts the injection process. The variation observed for 0 < [TBP] < 0.5 M is in agreement with existing studies showing that more basic electrolytes (with higher *tert*-butylpyridine concentrations) reduce J_{sc} while increasing V_{oc} [19]. The improved injection performance is clearly visible in the IPCE (Fig. 9-**right**). For instance, in the absence of *tert*-butylpyridine and with a 0.1 M Li^+ concentration, the highest J_{sc} value was achieved (56 % higher than the initial value), showing that the combination of both Li^+/*tert*-butylpyridine additives in a 0.1/0 ratio achieves higher injection performance than that obtained with the traditional 0.1/0.5 electrolyte. The absence of *tert*-butylpyridine allowed us to achieve an $IPCE_{max}$ value of 55 %, much higher than that obtained with a concentration of 0.5 M ($IPCE_{max}$ = 20 %). The highest

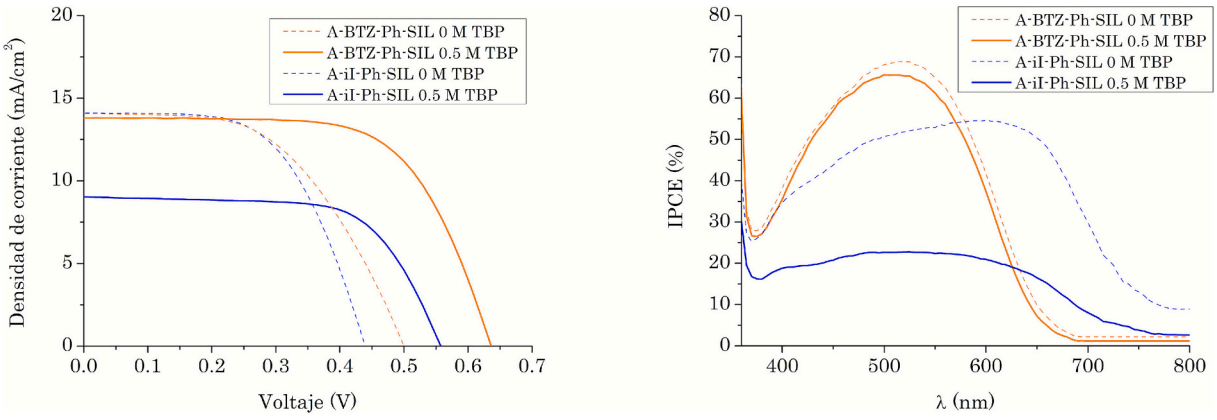

Fig. 7. *J/V* curves (left) and IPCE curve (right) with [TBP] = 0 M (⋯) and [TBP] = 0.5 M (—) of the dyes A-iI-Ph-SIL **(blue)** and A-BTZ-Ph-SIL **(orange).** 6 μm thick photoanode. (For interpretation of the references to color in this figure legend, the reader is referred to the web version of this article.)

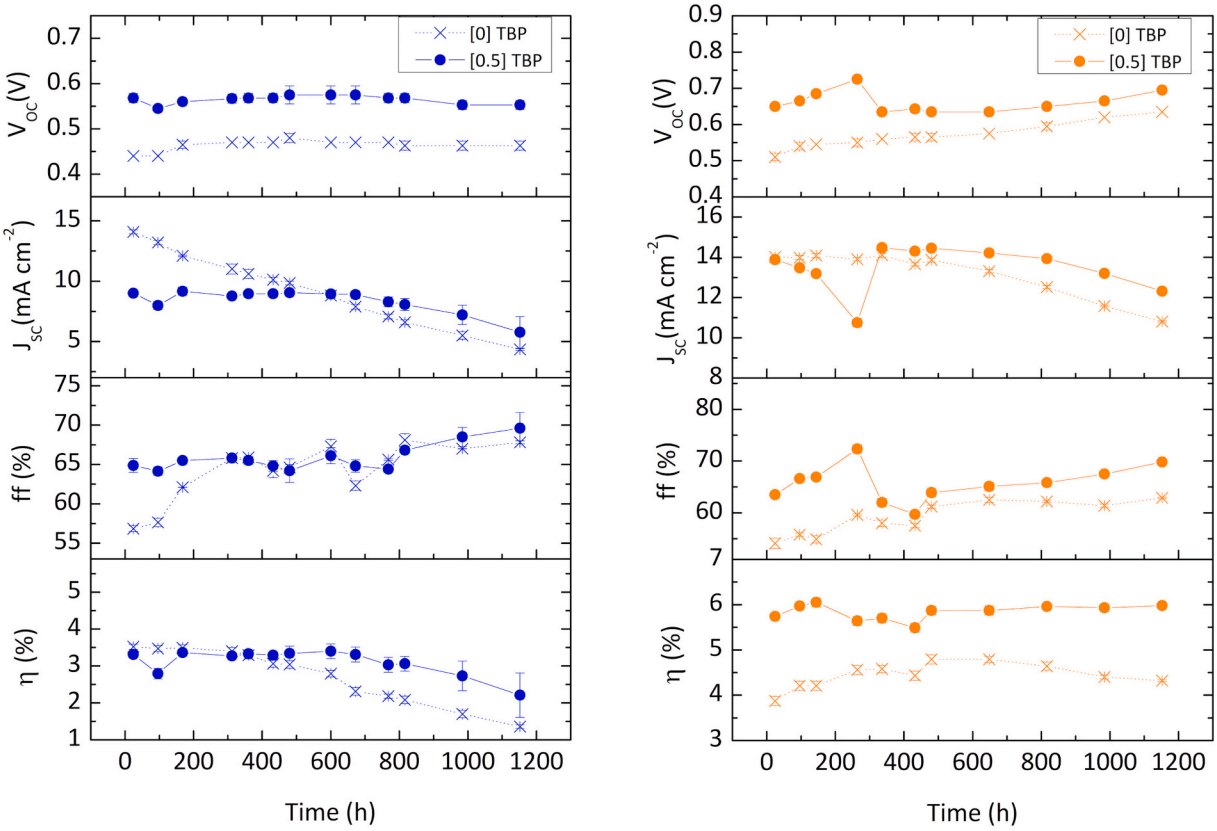

Fig. 8. Time evolution of the photovoltaic parameters for A-iI-Ph-SIL DSSCs (left) with [TBP] = 0 M (Blue ×) and [TBP] = 0.5 M (Blue ●). A-BTZ-Ph-SIL DSSCs (right) with [TBP] = 0 M (Orange ×) and [TBP] = 0.5 M (Orange ●). (For interpretation of the references to color in this figure legend, the reader is referred to the web version of this article.)

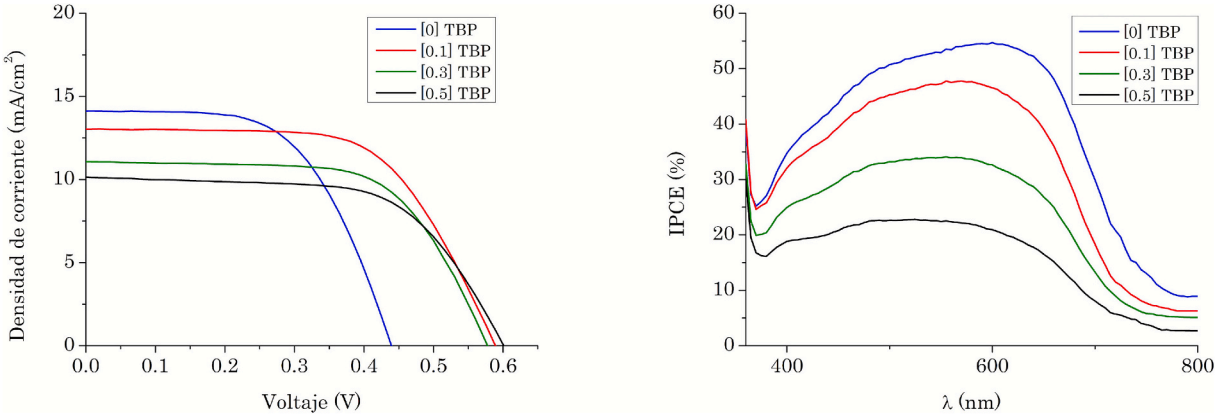

Fig. 9. *J/V* curves (left). IPCE curves (right) of the A-iI-Ph-SIL dye with different *tert*-butylpyridine concentrations.

efficiency (η = 4.79 %) was achieved with a 0.1 M *tert*-butylpyridine (TBP) concentration. This optimal concentration represents the ideal trade-off between the obtained J_{sc} and V_{oc} values, leading to a remarkable 44 % improvement over the initial efficiency.

3.6. EIS analysis

The charge transfer and electron transport processes were investigated using electrochemical impedance spectroscopy (EIS). The Nyquist and Bode plots for A-iI-Ph-SIL-based cells obtained under 1 SUN illumination are shown in Fig. 10.

The Nyquist plots (Fig. 10-**left**) for these DSSCs exhibit a shape that is common for such devices. Here, the radius of the intermediate semicircle is typically related to the recombination resistance (R_{rec}) at the TiO_2/dye/electrolyte interface. A larger R_{rec} value implies a reduction in recombination processes, which is known to result in a higher V_{oc}. In this study, the TBP-free electrolyte resulted in a clearly smaller semicircle radius compared to the other compositions. This is consistent with the lower V_{oc} of approximately 440 mV recorded for these cells. This type of effect has been reported to be related to the electron transfer kinetics [44]. In contrast, the addition of TBP led to much higher V_{oc} values, ranging from 560 to 590 mV. Notably, the larger radius was observed for the [TBP] = 0.1 M composition, which resulted in the highest V_{oc} and the best overall performance.

Bode plots allow us to estimate the electron lifetime in the TiO_2 photoanode from the angular frequency of the maximum in the largest

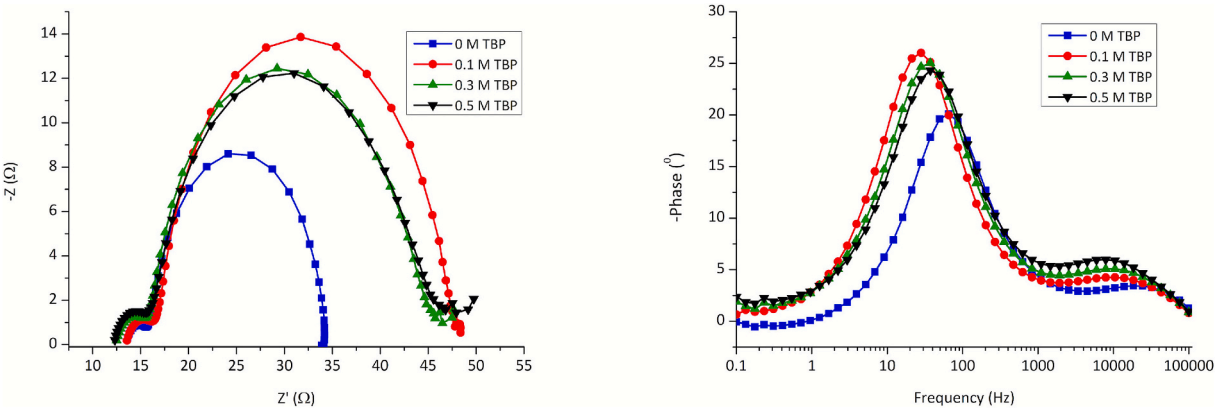

Fig. 10. EIS. Nyquist plot (left) and Body plot (right) of A-iI-Ph-SIL based DSSC devices. The effect of using electrolytes with different TBP concentration effects is shown.

impedance semicircle arc, which appears as a peak in the mid-frequency region [45]. In particular, in Fig. 10-**right**, the values of these electron lifetimes increase in this order of TBP concentration: 2.429 μs ([TBP] = 0 M), 4.269 μs ([TBP] = 0.3-0.5 M, 5.660 μs ([TBP] = 0.1 M). The longest electron lifetime corresponds with [TBP] = 0.1 M in the electrolyte and results in a V_{oc} = 590 mV, which constitutes the most effective suppression of the back electron transfer with the I_3^-/I^- mediator redox.

4. Conclusions

A new dye with a D-A'-π-A structure has been synthesized, using an alkylaniline as donor, D, and C5-chain-functionalized isoindigo as auxiliary acceptor, A'. The introduction of C5 chains into isoindigo via *N*-alkylation proved to be an effective strategy to prevent dye aggregation, offering an alternative to traditional anti-aggregants like CDCA, which showed no improvement in device efficiency.

The strength of the auxiliary acceptor greatly influences the thermodynamics of electron transfer and the proper distribution of electron density within the orbitals. The strong acceptor character of isoindigo in A-iI-Ph-SIL hindered efficient charge transfer from the donor to the acceptor. In contrast, benzothiadiazole, BTZ, a moderately strong acceptor, facilitated charge movement throughout the analogous A-BTZ-Ph-SIL molecule. In particular, for the A-iI-Ph-SIL dye, where efficient charge injection into the semiconductor was compromised due to a lower LUMO orbital energy, we found that the concentration of *tert*-butylpyridine in the electrolyte played a crucial role. Reducing the *tert*-butylpyridine content in the electrolyte shifts the TiO_2 conduction band edge towards positive values, thereby enhancing the injection process and consequently boosting the photocurrent. An optimal TBP concentration of 0.1 M led to a remarkable 44 % improvement in efficiency for devices using A-iI-Ph-SIL, achieving a maximum value of η = 4.79 % by striking the right balance between short-circuit current and open-circuit voltage.

Overall, our findings suggest that utilizing a moderate auxiliary acceptor in sensitizers is more convenient than the use of one with a strong character. This, along with the value of the oxidation potential of the excited state providing a sufficient driving force, ensures adequate electron injection into the semiconductor minimizing voltage losses. Consequently, dyes featuring moderate auxiliary acceptors, like A-BTZ-Ph-SIL, prove to be more suitable candidates for D-A'-π-A sensitizers in DSSC devices.

CRediT authorship contribution statement

Isolda Duerto: Data curation, Visualization, Writing – original draft. **Jesús Orduna:** Conceptualization, Formal analysis, Methodology, Supervision, Validation. **Belén Villacampa:** Formal analysis, Methodology, Validation, Writing – original draft, Writing – review & editing. **María-Jesús Blesa:** Conceptualization, Formal analysis, Methodology, Supervision, Validation, Writing – original draft, Writing – review & editing.

Declaration of competing interest

The authors declare that they have no known competing financial interests or personal relationships that could have appeared to influence the work reported in this paper.

Acknowledgements

The authors thank the financial support from Spain MCIN/AEI/10.13039/501100011033 (Project PID2019-104307 GB-I00), Grant CEX2023-001286-S funded by MICIU/AEI /10.13039/501100011033 and Gobierno de Aragón-Fondo Social Europeo (E47-23R) and also from Universidad de Zaragoza (UZ2023-CIE-01). ID acknowledge for the financial support of DGA fellowship program. The authors are grateful to D. Barrios for the help provided in the assembly of DSSCs and also would like to acknowledge the use of Servicio General de Apoyo a la Investigación-SAI, Universidad de Zaragoza. This research made use of Marvin, a core Python package and web framework for MaNGA data, developed by Brian Cherinka, José Sánchez-Gallego, Brett Andrews, and Joel Brownstein. (MaNGA Collaboration, 2018).

Appendix A. Supplementary data

Supplementary data to this article can be found online at https://doi.org/10.1016/j.jelechem.2025.119686.

Data availability

Data will be made available on request.

References

[1] H. Meddeb, M. Götz-Köhler, N. Neugebohrn, U. Banik, N. Osterthun, O. Sergeev, D. Berends, C. Lattyak, K. Gehrke, M. Vehse, Tunable photovoltaics: adapting solar cell technologies to versatile applications, Adv. Energy Mater. 12 (2022) 2200713, https://doi.org/10.1002/aenm.202200713.

[2] R. Jiang, H. Michaels, N. Vlachopoulos, M. Freitag, Chapter 8 - beyond the limitations of dye-sensitized solar cells, in: M. Soroush, K.K.S. Lau (Eds.), Dye-Sensitized Solar Cells, Academic Press, 2019, pp. 285–323, https://doi.org/10.1016/B978-0-12-814541-8.00008-2.

[3] Y. Gao, X. Li, Y. Hu, Y. Fan, J. Yuan, N. Robertson, J. Hua, S.R. Marder, Effect of an auxiliary acceptor on D-A-π-A sensitizers for highly efficient and stable dye-sensitized solar cells, J. Mater. Chem. A 4 (2016) 12865–12877, https://doi.org/10.1039/C6TA05588E.

[4] L. Huang, P. Ma, G. Deng, K. Zhang, T. Ou, Y. Lin, M.S. Wong, Novel electron-deficient quinoxalinedithienothiophene- and phenazinedithienothiophene-based photosensitizers: the effect of conjugation expansion on DSSC performance, Dyes Pigments 159 (2018) 107–114, https://doi.org/10.1016/j.dyepig.2018.06.010.

[5] D.H. Lee, M.J. Lee, H.M. Song, B.J. Song, K.D. Seo, M. Pastore, C. Anselmi, S. Fantacci, F. De Angelis, M.K. Nazeeruddin, M. Grätzel, H.K. Kim, Organic dyes incorporating low-band-gap chromophores based on π-extended benzothiadiazole for dye-sensitized solar cells, Dyes Pigments 91 (2011) 192–198, https://doi.org/10.1016/j.dyepig.2011.03.015.

[6] Y. Xie, H. Zhou, S. Zhang, C. Ge, S. Cheng, Influence of the auxiliary acceptor and π-bridge in triarylamine dyes on dye-sensitized solar cells, Photochem. Photobiol. Sci. 18 (2019) 2042–2051, https://doi.org/10.1039/c9pp00188c.

[7] I. Duerto, E. Colom, J.M. Andrés-Castán, S. Franco, J. Garín, J. Orduna, B. Villacampa, M.J. Blesa, DSSCs based on aniline derivatives functionalized with a *tert*-butyldimethylsilyl group and the effect of the pi-spacer, Dyes Pigm 148 (2018) 61–71, https://doi.org/10.1016/j.dyepig.2017.07.063.

[8] J.S. Ni, Y.C. Yen, J.T. Lin, Organic dyes with a fused segment comprising benzotriazole and thieno[3,2-b]pyrrole entities as the conjugated spacer for high performance dye-sensitized solar cells, Chem. Commun. 51 (2015) 17080–17083, https://doi.org/10.1039/C5CC07105D.

[9] S. Chaurasia, J.S. Ni, W.I. Hung, J.T. Lin, 2*H*-[1,2,3]Triazolo[4,5-c]pyridine cored organic dyes achieving a high efficiency: a systematic study of the effect of different donors and spacers, ACS Appl. Mater. Interfaces 7 (2015) 22046–22057, https://doi.org/10.1021/acsami.5b07205.

[10] J.K. Roy, R. Kaur, A. Daniel, A. Baumann, Q. Li, J.H. Delcamp, J. Leszczynski, Photophysical properties of donor-acceptor-π-bridge-acceptor sensitizers with a naphthobisthiadiazole auxiliary acceptor: toward longer-wavelength access in dye-sensitized solar cells, J. Phys. Chem. C 126 (2022) 11875–11888, https://doi.org/10.1021/acs.jpcc.2c02117.

[11] R. Stalder, J. Mei, K.R. Graham, L.A. Estrada, J.R. Reynolds, Isoindigo, a versatile electron-deficient unit for high-performance organic electronics, Chem. Mater. 26 (2014) 664–678, https://doi.org/10.1021/cm402219v.

[12] M.A. Kolaczkowski, B. He, Y. Liu, Stepwise bay annulation of indigo for the synthesis of desymmetrized electron acceptors and donor-acceptor constructs, Org. Lett. 18 (2016) 5224–5227, https://doi.org/10.1021/acs.orglett.6b02504.

[13] A. Yassin, P. Leriche, M. Allain, J. Roncali, Donor-acceptor-donor (D-A-D) molecules based on isoindigo as active material for organic solar cells, New J. Chem. 37 (2013) 502–507, https://doi.org/10.1039/C2NJ40879A.

[14] W. Ying, F. Guo, J. Li, Q. Zhang, W. Wu, H. Tian, J. Hua, Series of new D-A-π-A organic broadly absorbing sensitizers containing isoindigo unit for highly efficient dye-sensitized solar cells, ACS Appl. Mater. Interfaces 4 (2012) 4215–4224, https://doi.org/10.1021/am300925e.

[15] W. Gang, T. Haijun, Z. Yiping, W. Yingying, H. Zhubin, Y. Guipeng, P. Chunyue, Series of D-π-a system based on isoindigo dyes for DSSC: synthesis, electrochemical and photovoltaic properties, Synth. Met. 187 (2014) 17–23, https://doi.org/10.1016/j.synthmet.2013.09.039.

[16] D. Wang, W. Ying, X. Zhang, Y. Hu, W. Wu, J. Hua, Near-infrared absorbing isoindigo sensitizers: synthesis and performance for dye-sensitized solar cells, Dyes Pigments 112 (2015) 327–334, https://doi.org/10.1016/j.dyepig.2014.07.017.

[17] C. Liao, H. Wu, H. Tang, L. Wang, D. Cao, Expanding π-bridge and introducing auxiliary acceptor for realizing panchromatic absorption of the phenothiazine dyes in dye-sensitized solar cells, Sol. Energy 240 (2022) 399–407, https://doi.org/10.1016/j.solener.2022.05.043.

[18] V. Suryanarayanan, K.-M. Lee, J.-G. Chen, K.-C. Ho, High performance dye-sensitized solar cells containing 1-methyl-3-propyl imidazolinium iodide-effect of additives and solvents, J. Electroanal. Chem. 633 (2009) 146–152, https://doi.org/10.1016/j.jelechem.2009.05.005.

[19] S.E. Koops, B.C. O'Regan, P.R. Barnes, J.R. Durrant, Parameters influencing the efficiency of electron injection in dye-sensitized solar cells, J. Am. Chem. Soc. 131 (2009) 4808–4818, https://doi.org/10.1021/ja8091278.

[20] M. Liang, J, Chen, Arylamine organic dyes for dye-sensitized solar cells, Chem. Soc. Rev. 42 (2013) 3453–3488, https://doi.org/10.1039/c3cs35372a.

[21] M. González-Lainez, M.T. Jiménez-Ruiz, N. Martínez De Baroja, J. Garín, J. Orduna, B. Villacampa, M.J. Blesa, Using functionalized non-linear optical chromophores to prepare NLO-active polycarbonate films, Dyes Pigments 119 (2015) 30–40, https://doi.org/10.1016/j.dyepig.2015.02.026.

[22] M.A. Cerdán-Bernad, Nuevos sistemas push-pull orgánicos y metaloorgánicos derivados de ditiafulveno y sistemas isoelectrónicos, Ph.D. Thesis,, Universidad de Zaragoza, 2008.

[23] S. Haid, M. Marszalek, A. Mishra, M. Wielopolski, J. Teuscher, J.E. Moser, R. Humphry-Baker, S.M. Zakeeruddin, M. Grätzel, P. Bäuerle, Significant improvement of dye-sensitized solar cell performance by small structural modification in π-conjugated donor-acceptor dyes, Adv. Funct. Mater. 22 (2012) 1291–1302, https://doi.org/10.1002/adfm.201102519.

[24] J. Mei, K.R. Graham, R. Stalder, J.R. Reynolds, Synthesis of isoindigobased oligothiophenes for molecular bulk heterojunction solar cells, Org. Lett. 12 (2010) 660–663, https://doi.org/10.1021/ol902512x.

[25] A. Leliège, C.H.L. Régent, M. Allain, P. Blanchard, J. Roncali, Structural modulation of internal charge transfer in small molecular donors for organic solar cells, Chem. Commun. 48 (2012) 8907–8909, https://doi.org/10.1039/C2CC33921H.

[26] E. Knoevenagel, "condensation von Malonsäure mit aromatischen Aldehyden durch Ammoniak und amine" [condensation of malonic acid with aromatic aldehydes via ammonia and amines], Ber. Dtsch. Chem. Ges. 31 (1898) (1898) 2596–2619, https://doi.org/10.1002/cber.18980310308.

[27] S. Krishnan, K. Senthilkumar, The influence of the shape and configuration of sensitizer molecules on the efficiency of DSSCs: a theoretical insight, RSC Adv. 11 (2021) 5556–5567, https://doi.org/10.1039/D0RA10613E.

[28] J.N. Clifford, E. Martínez-Ferrero, A. Viterisi, E. Palomares, Sensitizer molecular structure-device efficiency relationship in dye sensitized solar cells, Chem. Soc. Rev. 40 (2011) 1635–1646, https://doi.org/10.1039/B920664G.

[29] A. Amkassou, H. Zgou, DFT and TD-DFT study of new D-π-a dyes for Grätzel solar cell, AIP Conf. Proc. 2056 (2018), https://doi.org/10.1063/1.5084976.

[30] A.E. Reed, R.B. Weinstock, F. Weinhold, Natural population analysis, J. Chem. Phys. 83 (1985) 735–746, https://doi.org/10.1063/1.449486.

[31] H. Roohi, N. Mohtamadifar, The role of the donor group and electronaccepting substitutions inserted in π-linkers in tuning the optoelectronic properties of D-π-a dye-sensitized solar cells: a DFT/TDDFT study, RSC Adv. 12 (2022) 11557–11573, https://doi.org/10.1039/D2RA00906D.

[32] S. Trabelsi, N. Kouki, M. Seydou, F. Maurel, B. Tangour, Intramolecular path determination of active electrons on push-pull oligocarbazole dyes-sensitized solar cells, ChemistryOpen 8 (2019) 580–588, https://doi.org/10.1002/open.201800224.

[33] N. Gao, X. Lin, J. Liu, Y. Li, Y. Yang, Photoactuated properties of acetylene congeners non-metallic dyes and molecular design for solar cells, Materials 11 (2018) 2027, https://doi.org/10.3390/ma11102027.

[34] S. Ahmed, S.R. Bora, T. Chutia, D.J. Kalita, Structural modulation of phenothiazine and coumarin based derivatives for high performance dye sensitized solar cells: a theoretical study, Phys. Chem. Chem. Phys. 23 (2021) 13190–13203, https://doi.org/10.1039/D1CP00036E.

[35] M. Mirzaei, M.B. Gholivand, P-doped NiS_2/Ni nanoheteroparticles embedded into N-doped carbon framework anchored on multi-walled carbon nanotubes as an efficient counter electrode for Pt-free dye-sensitized solar cells, Mater. Today Chem. 35 (2024) 101862, https://doi.org/10.1016/j.mtchem.2023.101862.

[36] S. Zhang, X. Yang, K. Zhang, H. Chen, M. Yanagida, L. Han, Effects of 4-*tert*-butylpyridine on the quasi-Fermi levels of TiO_2 films in the presence of different cations in dye-sensitized solar cells, Phys. Chem. Chem. Phys. 13 (2011) 19310–19313, https://doi.org/10.1039/C1CP22832C.

[37] S.G. Li, K.J. Jiang, J.H. Huang, L.M. Yang, Y.L. Song, Molecular engineering of panchromatic isoindigo sensitizers for dye-sensitized solar cell applications, Chem. Commun. 50 (2014) 4309–4311, https://doi.org/10.1039/D1CP00036E.

[38] C. Aumaitre, C. Rodriguez-Seco, J. Jover, O. Bardagot, F. Caffy, Y. Kervella, N. López, E. Palomares, R. Demadrille, Visible and near-infrared organic photosensitizers comprising isoindigo derivatives as chromophores: synthesis, optoelectronic properties and factors limiting their efficiency in dye solar cells, J. Mater. Chem. A 6 (2018) 10074–10084, https://doi.org/10.1039/C8TA01826J.

[39] G. Boschloo, L. Häggman, A. Hagfeldt, Quantification of the effect of 4-*tert*-butylpyridine addition to I–/I3 – redox electrolytes in dye-sensitized nanostructured TiO_2 solar cells, J. Phys. Chem. B 110 (2006) 13144–13150, https://doi.org/10.1021/jp0619641.

[40] S. Paek, H. Choi, C. Kim, N. Cho, S. So, K. Song, M.K. Nazeeruddin, J. Ko, Efficient and stable panchromatic squaraine dyes for dye-sensitized solar cells, Chem. Commun. 47 (2011) 2874, https://doi.org/10.1039/c0cc05378c.

[41] J. Park, G. Viscardi, C. Barolo, N. Barbero, Near-infrared sensitization in dye sensitized solar cells, Chimia 67 (2013) 129–135, https://doi.org/10.2533/chimia.2013.129.

[42] B. Liu, X. Li, M. Liu, Z. Ning, Q. Zhang, C. Li, K. Müllen, W. Zhu, Photovoltaic performance of solid-state DSSCs sensitized with organic isophorone dyes: effect of dye-loaded amount and dipole moment, Dyes Pigments 94 (2012) 23–27, https://doi.org/10.1016/j.dyepig.2011.11.005.

[43] G.G. Sonai, A. Tiihonen, K. Miettunen, P.D. Lund, A.F. Nogueira, Long-term stability of dye-sensitized solar cells assembled with cobalt polymer gel electrolyte, J. Phys. Chem. C 121 (2017) 17577–17585, https://doi.org/10.1021/acs.jpcc.7b03865.

[44] G.G. Köse, G.K. Karaoğlan, Y.E. Maden, A. Koca, Influence of 2-naphthoic acid anchoring groups to the photovoltaic performance of zinc phthalocyanine-based photosensitizers in dye-sensitized solar cell, J. Electroanal. Chem. 945 (2023) 117691, https://doi.org/10.1016/j.jelechem.2023.117691.

[45] X. Tang, Y. Wang, G. Cao, Effect of the adsorbed concentration of dye on charge recombination in dye-sensitized solar cells, J. Electroanal. Chem. 694 (2013) 6–11, https://doi.org/10.1016/j.jelechem.2013.01.036.